Surface Film Formation and Lithium Underpotential Deposition on Au(111) Surfaces in Propylene Carbonate : In Situ Scanning Tunneling Microscopy Study

Toshiya Saito and Kohei Uosaki

J. Electrochem. Soc. 2003, Volume 150, Issue 4, Pages A532-A537.
doi: 10.1149/1.1557966

Journal of The Electrochemical Society, **150** (4) A532-A537 (2003)
0013-4651/2003/150(4)/A532/6/$7.00 © The Electrochemical Society, Inc.

Surface Film Formation and Lithium Underpotential Deposition on Au(111) Surfaces in Propylene Carbonate

In Situ Scanning Tunneling Microscopy Study

Toshiya Saito and Kohei Uosaki*,z

Physical Chemistry Laboratory, Division of Chemistry, Graduate School of Science, Hokkaido University, Sapporo 060-0810, Japan

The formation and the morphological change of surface film on a Au(111) electrode in propylene carbonate solution containing 0.1 M $LiClO_4$ in the potential region between 0.8 and 2.5 V (Li/Li^+) were studied by *in situ* scanning tunneling microscopy. The surface film was observed on a gold electrode at potentials more negative than 1.5 V (Li/Li^+), and many nuclei appeared on the flat terrace of the electrode at potentials more negative than 0.9 V, where underpotential deposition of lithium on gold was started. Many holes on the surface film were observed after the dissolution of lithium and were thought to be formed as a result of breakdown of the film in nanometer order. The deposition and dissolution of the submonolayer lithium affected the surface morphology in nanometer order.
 [DOI: 10.1149/1.1557966]

Manuscript submitted June 7, 2002; revised manuscript received September 9, 2002. Available electronically March 6, 2003.

Introduction

The electrochemical deposition and dissolution of lithium in aprotic solvents has attracted much attention because of the industrial significance with regard to application in lithium secondary batteries. Although lithium metal is the ideal material as an anode of light weight and small-size rechargeable batteries,[1] the lower reversibility of the lithium deposition/dissolution cycle than that of the lithium intercalation/deintercalation cycle at a carbon electrode inhibits practical application of lithium metal for secondary batteries.

Due to the high reactivity of lithium metal, the lithium electrode is known to be always covered by a surface film in an aprotic solvent. The solid electrolyte interphase (SEI) model[2,3] is the most accepted to describe this film. In this model, the film is thought to have lithium ion conductivity, and the deposition and dissolution of lithium take place at the film/electrode interface so that reactions between lithium and the solvent and/or anion are prevented. Thus, the physical and chemical properties of the surface film significantly affect the electrochemical properties of the lithium electrode. For example, nonuniformity of the surface film such as thickness distribution induces nonuniform current distribution on a lithium electrode and causes growth of dendrites.[4,5] The ''breakdown and repair'' mechanism was proposed by Dey and Schlaikjer, explaining the behavior of the surface film during the dissolution of lithium.[6] According to their proposal, a part of the surface film becomes cracked during the dissolution of lithium. The exposed lithium at the bottom of the cracked hole reacts with the solvent and/or anion and the surface film is formed within the cracked hole. As a result of the ''breakdown and repair,'' the surface film becomes inhomogeneous because the original film and the repaired film may have different chemical and physical properties. Actually, the roughening of the surface after the dissolution of lithium was confirmed by *in situ* atomic force microscopy (AFM).[7] The growth of dendrites and/or breakdown of the film on the lithium electrode should be responsible for the low reversibility of the lithium deposition/dissolution cycle and may cause electric shorts or the isolation of metallic lithium. Morphological changes of the lithium surface were already observed under various conditions by scanning electron microscopy (SEM) and AFM.[4,7-12] The control of the chemical and physical properties of the surface film is an important subject for the development of lithium secondary batteries.

Aurbach *et al.* reported the heterogeneity in the surface film on the lithium electrode by *in situ* AFM and lateral force microscopy,[7,13] suggesting that the lithium deposition preferentially proceeds at a specific site on the surface such as a place where the film is thinner than other parts. Shiraishi *et al.* also found that dendritic lithium was covered with a thinner surface film than other places by using surface potential microscopy and suggested that higher current flow at the site with thinner film promotes the growth of dendritic lithium.[14]

The *in situ* investigations carried out so far were, however, limited in the order of micrometers or submicrometers at most, and the mechanism of morphological change of the surface film such as breakdown in nanometer scale was still unknown. One of the main reasons for the lack of surface investigation with nanometer resolution is the difficulty in the preparation of a well-ordered lithium surface.

Although noble metals and transition metals are less reactive than alkali metals, the reduction of the solution components leading to film formation is reported to take place even on noble or transition metal electrode in the relatively negative potential region.[15-17] This process can be considered as model reaction for the surface film formation on a lithium electrode. The surface films formed on nickel and gold electrodes in propylene carbonate (PC) solution were reported to be composed of several layers, which are roughly divided into two parts, namely, a compact layer at the metal side and a porous layer at the solution side.[17,18] The compact layer is composed of LiOH and/or Li_2CO_3, and the porous layer contains some organic components.[17,18] Since it is much easier to prepare a well-defined and clean surface of noble metal, it is appropriate to use the noble meal electrode to investigate the fundamental process of surface film and lithium deposition/dissolution in nonaqueous solutions.

We have already examined the surface morphology of a Au(111) electrode in PC solution containing 0.1 M $LiClO_4$ by *in situ* STM at potentials between 1.9 and 2.5 V where no faradaic current flowed.[19] We found that the surface of the Au(111) electrode was covered with an ultrathin film whose structure changed with applied potentials. An island-like adsorbate was observed at potentials more positive than the potential of zero charge (pzc), and a flat smooth surface having small holes of several nanometers was observed at potentials more negative than the pzc.

In this study, we extended the *in situ* electrochemical scanning tunneling microscopy (STM) observation of the Au(111) electrode in PC solution containing 0.1 M $LiClO_4$ to the more negative potential region where the reduction processes including underpotential deposition (UPD) of lithium take place. The surface film formation and morphological change of the film as a function of the electrode potential are discussed based on the STM observation as well as the results of cyclic voltammetry (CV).

* Electrochmeical Society Active Member.
z E-mail: uosaki@pcl.sci.hokudai.ac.jp

Experimental

A gold single-crystal bead was prepared by Clavilier's method[20] from a gold wire (Tanaka Precious Metal, 99.99% purity) and was cut parallel to a (111) facet. The exposed (111) face was polished with a diamond slurry down to 0.5 μm. The crystal was then annealed in an electric furnace at 850°C for 12 h under an argon atmosphere. Lithium wire (Johnson-Matthey, 99.9% purity) was cut and washed several times with hexane in an argon-filled glove box (VAC, Nexus 2000 system) before use as a reference electrode. Platinum wire (Tanaka Precious Metal, 99.99% purity) was used as a counter electrode. PC solution containing 0.1 M $LiClO_4$ was purchased from Tomiyama Chemicals (lithium battery grade). The solution contained less than 20 ppm water and was stored in the glove box to avoid the dissolution of water or oxygen into the solution and was used without further purification. The electrode potentials are referenced with respect to the lithium reference electrode.

The STM measurement was carried out in the argon-filled glove box using a Nanoscope E control unit (Digital Instruments) and a PicoSPM scanning unit (Molecular Imaging) with a homemade electrochemical cell made of poly(chlorotrifluoroethylene) (PCTFE). The STM tip was mechanically cut 20% Ir-Pt wire (ϕ = 0.3 mm) coated with Apiezon wax. The scanning unit and a homemade vibration isolator were placed in the glove box, while the control unit was placed outside the glove box. The scanning unit was electronically connected to the control unit through an airtight connector. Prior to STM measurement, the gold single crystal was annealed by a gas flame for a few min and cooled under argon gas stream. The annealed gold substrate was transferred to the glove box as kept in a hexane-filled glass container. The gold single crystal was then fixed on the electrochemical STM cell. Argon gas in the glove box was circulated through catalysts to remove oxygen and water. The oxygen concentration in the glove box was kept below 1 ppm, typically 0.1-0.2 ppm. The dew-point temperature in the glove box was less than the lower limit of the hygrometer, *i.e.*, below −100°C. The blower for argon circulation and a vacuum pump for controlling the inner pressure of the glove box were stopped during the STM measurement. The oxygen concentration in the glove box was a few ppm, at most 5 ppm, even 12 h after the STM experiment without any argon circulation. The water concentration was still under the lower limit of the hygrometer after the STM measurement.

Cyclic voltammetry was carried out using a three-compartment glass cell in the glove box while argon was continuously circulated. The electrochemical potential was controlled by a potentiostat (Hokuto Denko, HA-151), and the external potential was provided by a function generator (Hokuto Denko, HB-111). The potentiostat and the function generator were placed outside the glove box and were electronically connected to the electrochemical cell through an airtight connector. The annealing and transfer procedures of the gold electrode were the same as for the STM measurement.

Results and Discussion

Electrochemical characteristics.—Figure 1 shows a CV of the Au(111) electrode in PC solution containing 0.1 M $LiClO_4$. The rest potential of the electrode was about 2.8 V, and the first potential scan (Fig. 1a) was initiated from this potential at a scan rate of 50 mV/s. The potential was reversed at 0.2 V and was scanned between 0.2 and 2.09 V, which is the pzc of the Au(111) electrode in this solution as previously reported,[19] in the following cycles. The results of the second cycle and of a cycle after a continuous scan for 10 min, *i.e.*, of a steady state, are shown in Fig. 1b and c, respectively. The positions of the cathodic peaks and value of the cathodic current in the first and second negative-going potential scans in the potential region of 0.5-2.0 V were very similar to those of the previous result, in which the electrode potential was scanned between 0.5 and 2.5 V.[19] In the first scan, three cathodic peaks appeared at 1.5, 0.9, and 0.35 V, and the current rapidly decreased as the potential was scanned to a more negative value. After reversing the potential scan at 0.2 V, the current became anodic at 0.6 V, reached a peak at *ca.* 1.1 V, and then decreased as the potential became more positive.

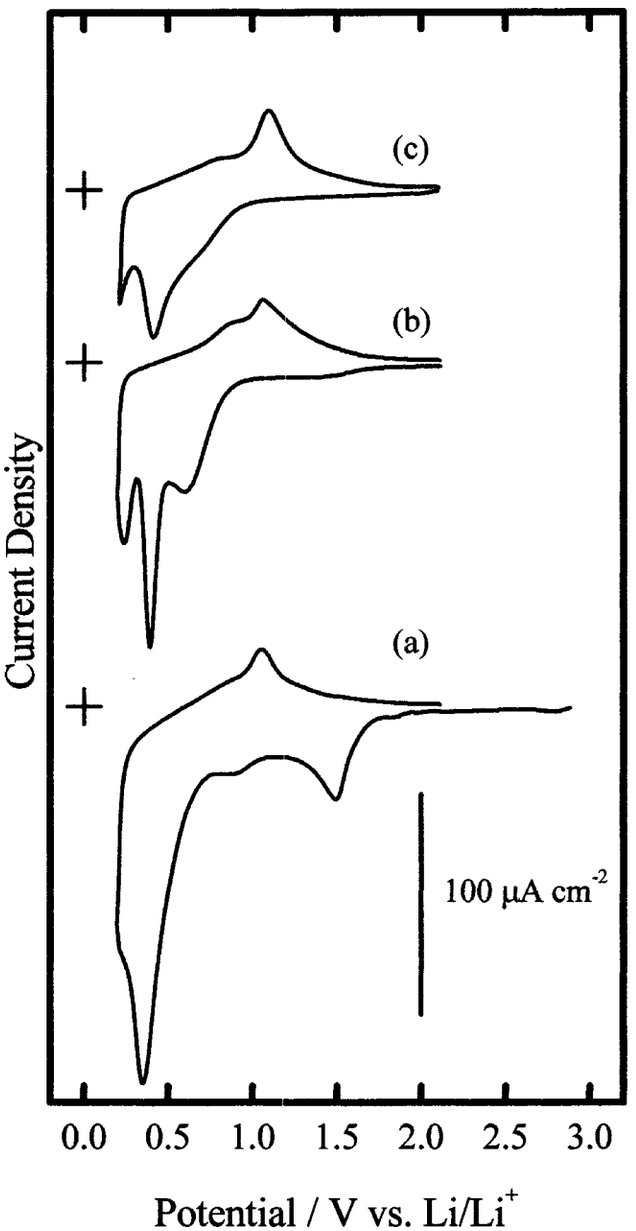

Figure 1. Cyclic voltammogram of Au(111) electrode in the PC solution containing 0.1 M $LiClO_4$ at 50 mV/s. The rest potential of the electrode was *ca.* 2.8 V, and (a) the first potential scan was initiated from this potential at a scan rate of 50 mV/s. The potential was reversed at 0.2 V and was scanned between 0.2 and 2.09 V in (b) the second cycle and (c) the cycle after continuous scan for 10 min, *i.e.*, as the steady state.

In the second negative-going scan, three new peaks were observed at 0.6, 0.4, and 0.25 V. In the following positive-going scan, the current changed to anodic at 0.4 V, which was more negative than the value in the first scan. In addition to the anodic peak at *ca.* 1.1 V, a small shoulder at *ca.* 0.9 V, which was not observed in the first scan, was observed. The peak current of the anodic peak at *ca.* 1.1 V was slightly larger than that of the first scan.

In the steady-state scan (Fig. 1c), the cathodic current in the negative-going scan was smaller than those in the first and the second scans, and that at 0.4 V was 67 μA/cm^2. The cathodic peak at

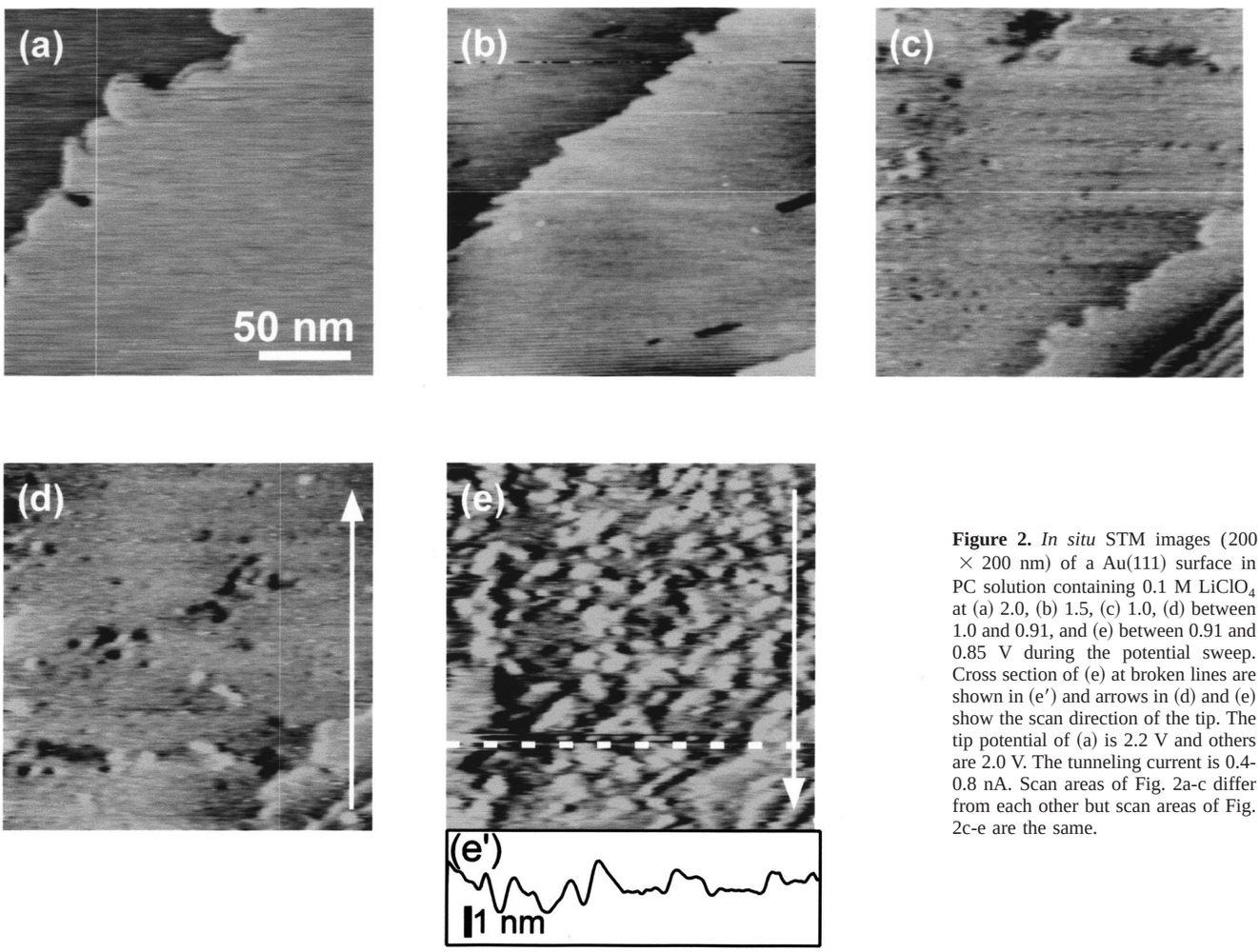

Figure 2. *In situ* STM images (200 × 200 nm) of a Au(111) surface in PC solution containing 0.1 M $LiClO_4$ at (a) 2.0, (b) 1.5, (c) 1.0, (d) between 1.0 and 0.91, and (e) between 0.91 and 0.85 V during the potential sweep. Cross section of (e) at broken lines are shown in (e′) and arrows in (d) and (e) show the scan direction of the tip. The tip potential of (a) is 2.2 V and others are 2.0 V. The tunneling current is 0.4-0.8 nA. Scan areas of Fig. 2a-c differ from each other but scan areas of Fig. 2c-e are the same.

around 0.6 V was significantly decreased and was observed only as a shoulder. The cathodic peak at 0.25 V observed in the second scan shifted negatively as the scan was repeated and was not observed in the steady state. The anodic peak at *ca.* 1.1 V became larger with the peak current of 36 $\mu A/cm^2$. The cathodic shoulder at *ca.* 0.8 V became smaller.

As we have already reported,[19] the cathodic current at *ca.* 1.5 V was thought to be due to the reduction of water, which was contained in the electrolyte solution as an impurity, and the absence of the cathodic peak at around 2.0 V shows that no oxygen was contained in the solution. The cathodic peaks between 0.4 and 0.6 V were assigned to UPD of lithium, although the reason why two peaks appeared is unclear.[15,21] The cathodic peak at more negative values than 0.3 V was considered to be due to alloy formation between lithium and gold.[15,21] The reduction of solvent and/or anion should also contribute to the cathodic current.[15] The anodic peak at *ca.* 1.1 V and a small shoulder at *ca.* 0.9 V were reported to be due to the dissolution of UPD lithium and lithium-gold alloy, respectively.[15,21]

The anodic peak at *ca.* 1.1 V was not observed when the negative-going potential scan was reversed at 0.8 V. The charge corresponding to the anodic peak, however, grew with the holding time at 0.8 V, and it took 2 min to reach a limiting value of *ca.* 55 $\mu C/cm^2$, which is about half the anodic charge calculated from the CV shown in Fig. 1c of 96 $\mu C/cm^2$. This result shows that lithium UPD on the Au(111) surface took place even at 0.8 V, although the deposition rate was rather slow. Scan rate dependence of CV showed that the cathodic peak shifted positively as the scan rate became slower. Cathodic current started to flow even at *ca.* 0.9 V when the scan rate was 1 mV/s. This result supports that lithium deposition can take place as positive as 0.8 V.

Morphological change of the surface during first potential scan.—Figures 2 and 3 show STM images of the Au(111) surface captured at various potentials. Figure 2a shows an STM image captured after the electrolyte solution was injected into the STM cell while keeping the potential of the gold electrode at 2.5 V and then the potential was stepped to 2.0 V. Two flat terraces separated by *ca.* 0.25 nm, *i.e.*, a monoatomic step of Au(111), were observed. No faradaic current flowed, indicating that a reduction reaction had not occurred yet. Thus, the surface film containing reduced products did not form yet, but a very thin adsorbate layer of the solvent was expected at this potential, as previously reported.[19]

The electrode potential was then swept negatively to 1.5 V at a scan rate of 1 mV/s. A cathodic current flowed and STM images became noisy during the potential sweep. Figure 2b shows an STM image captured at 1.5 V after the cathodic current significantly decreased. Holes *ca.* 0.5 nm deep were observed on the flat terraces.

The potential was swept negatively again from 1.5 to 1.0 V at 1 mV/s. The cathodic current also flowed and the STM image became noisy during the potential scan. Fig. 2c shows an STM image captured after the cathodic current significantly decreased. The terraces separated by a monoatomic, *i.e.*, 0.25 nm, step were still observed, but many holes of typically 0.5 nm deep and various diameters between several nanometers and several tens of nanometers were found on the terraces. The formation of the surface film on a noble

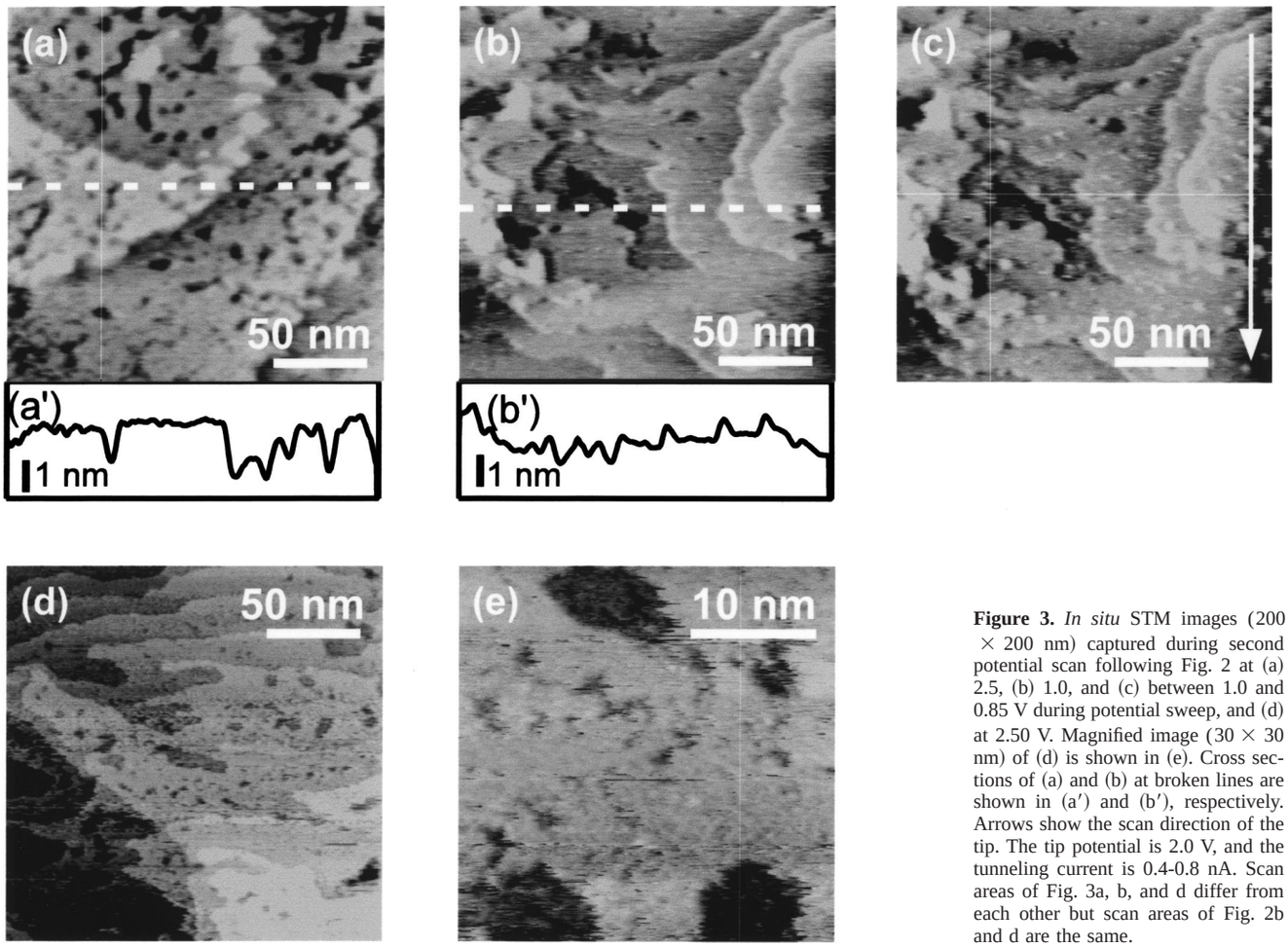

Figure 3. *In situ* STM images (200 × 200 nm) captured during second potential scan following Fig. 2 at (a) 2.5, (b) 1.0, and (c) between 1.0 and 0.85 V during potential sweep, and (d) at 2.50 V. Magnified image (30 × 30 nm) of (d) is shown in (e). Cross sections of (a) and (b) at broken lines are shown in (a′) and (b′), respectively. Arrows show the scan direction of the tip. The tip potential is 2.0 V, and the tunneling current is 0.4-0.8 nA. Scan areas of Fig. 3a, b, and d differ from each other but scan areas of Fig. 2b and d are the same.

metal electrode at potentials more negative than 1.5 V has been confirmed in several reports by using Fourier transform infrared (FTIR), X-ray photoelectron spectroscopy (XPS), electrochemical quartz crystal microbalance (EQCM), and surface-enhanced Raman scattering (SERS).[15,21-26] The dominant compositions of the surface film were considered as $ROCO_2Li$ and/or Li_2CO_3, which were produced as a result of the one- or two-electron reduction of the solvent.[17,18] Actually, the cathodic charge between 2.0 and 1.0 V in the first scan of CV (Fig. 1a) was *ca.* 400 $\mu C/cm^2$ and is sufficient to form the surface film covering the electrode surface of the gold electrode with the one- or two-electron reduction process. The surface shown in Fig. 2b should be covered by a surface film with a uniform thickness of *ca.* 0.5 nm containing the reduction product of the solvent, and the holes on the terraces should be defects in the surface film. It must be noted that although it was reported that the overlayer of the surface film formed on gold in PC solution containing $LiClO_4$ was porous by several groups,[17,27] the surface observed in the present study was rather smooth. This may be because the surface film of the present study was only 1 or 2 monolayers, while the films in the previous reports were much thicker due to a prolonged reduction.

The electrode potential was then scanned more negatively at 1 mV/s. Fig. 2d and e were captured during a negative potential scan from 1.0 to 0.91 V and from 0.91 to 0.85 V, respectively. Many nuclei appeared on the terrace when the electrode potential became more negative than *ca.* 0.9 V (Fig. 2e). The nuclei were several tens of nanometers in diameter and *ca.* 0.5-1 nm in height as presented in the cross section of the terrace shown by the broken line (Fig. 2e′). Although UPD of lithium took place at this potential as mentioned before, the nuclei height is too large for a lithium atom whose diameter is only 0.3 nm. Thus, the nuclei should be a morphological change of the surface film accompanied by lithium deposition. No clear image was obtained at potentials more negative than 0.85 V.

Surface morphology after dissolution of lithium.—The electrode potential was further scanned negatively and when the potential became 0.6 V, the potential was stepped to 2.5 V. Figure 3a shows an STM image captured at 2.5 V after the anodic current sufficiently decreased so that noise in the STM image became negligible. Many holes of several tens of nanometers in diameter were observed on the terraces. The surface became very rough compared with the surface before the lithium deposition (Fig. 2a). Worm-eaten holes of *ca.* 10 nm diam were observed everywhere on the terrace, and the number of steps increased compared to the surface shown in Fig. 2a. The step height and depth of the holes were roughly a multiple of 0.5 nm, as shown in the cross section at the broken line (Fig. 3a′). The EQCM measurement showed that the surface film formed on a gold electrode in PC solution containing $LiClO_4$ or $LiAsF_6$ at potentials more negative than 1.5 V did not dissolve even when the potential became as positive as 3.0 V.[23-25] The gold surface shown in Fig. 3a captured at 2.5 V is expected to be still covered with the surface film. There are two plausible reasons for the roughening of the surface after the dissolution of lithium. One is the morphological change of the surface film itself. In this case, the surface film was roughened during lithium dissolution, while the gold electrode beneath the film still remained flat. The other is the roughening of the gold surface covered with a film of uniform thickness.

Morphological change of the surface during the second negative potential scan.—The electrode potential was swept again to 1.0 V with 10 mV/s. Figure 3b shows an STM image captured at 1.0 V after the cathodic current significantly decreased. The hole density significantly decreased after the negative potential scan. The step heights of these terraces are *ca.* 0.25 nm as shown in Fig. 3b, and this value is close to the monoatomic step height of the Au(111) surface. Since no lithium deposition is expected in this potential region, the decrease in the hole density should be the result of the surface film formation. Actually, the surface film formation was reported to take place in this potential region during the several initial scans.[23-25] Thus, the worm-eaten holes observed in Fig. 3a are concluded to be the holes in the surface film, not in the gold. The film is probably broken by intensive flux of the lithium ion. Since the electrode surface is exposed to the electrolyte at the hole, the surface at the holes should be electrochemically more active than other places and therefore the reduction reaction of solvent and/or anion should selectively proceed at the bottom of the holes, resulting in filling of the holes by the reaction products.

As compared with Fig. 2, the number of step lines increased in Fig. 3b. This cannot be explained by the hole formation. The anodic shoulder of stripping lithium from the lithium-gold alloy was observed at 0.8 V, and the alloy formation dissolution cycle of lithium on gold is the probable reason for the generation of new steps on the gold.

Figure 3c shows an STM image during a potential sweep from 1.0 to 0.85 V with 5 mV/s. The nucleation on the terraces was observed and the nucleation density seems to become larger as the potentials became negative. Compared to the result of the first potential scan (Fig. 2e), the nucleation density in the same potential region (lower 70% of Fig. 3c) was smaller than that of the first potential cycle, but no obvious difference in size of the nuclei was found. The difference in the nucleation density between the first and the second potential cycles may reflect the difference in the densities of the surface defect.

The electrode potential was swept to 0.6 V and then stepped to 2.5 V. Figure 3d and e shows STM images of 200 × 200 nm and 30 × 30 nm, respectively, at 2.5 V after the second potential cycle. The surface structure was very similar to the one observed after the first lithium dissolution (Fig. 3a). The worm-eaten surface should be the result of the breakdown of the surface film as mentioned before. The surface structure did not change even after the potential was kept at 2.5 V for 30 min, in contrast to the result observed before the lithium deposition where the growth of the island structure was observed.[19] This result shows that the adsorbate layer on the bare gold surface was replaced by the surface film containing reduced products of the solution, and no adsorbate layer remained on the electrode surface based on the STM observation.

Conclusion

The surface film formation and lithium deposition process on a gold electrode can be schematically summarized in Fig. 4. At 2.0 V, no faradaic current flows and there is an adsorbate layer on the gold surface as previously reported (Fig. 4a).[19] A cathodic current flows and a surface film of uniform thickness is formed on the gold surface as the potential becomes more negative (Fig. 4b). When the electrode potential becomes more negative than 0.9 V, lithium deposition and further formation of the surface film simultaneously take place (Fig. 4c). The lithium deposition seems to proceed at the defect of the film and the film formation is further induced by the lithium deposition. When the electrode potential is stepped to 2.5 V, the dissolution of lithium takes place. The breakdown of the surface film in nanometer order is induced by the intensified flux of the lithium ion resulting in many worm-eaten holes of *ca.* 10 nm diam after the dissolution (Figs. 4d-e). The step density on the gold is increased maybe due to the alloy formation dissolution cycle. When the electrode potential is swept negatively again, the surface film formation predominantly takes place at the holes, resulting in the filling of the holes (Fig. 4f). Lithium deposition and further formation of the surface film simultaneously start again from *ca.* 0.9 V (Fig. 4g). The ''breakdown and repair'' process in nanometer order is repeated during the potential cycle of the electrode between 0.8 and 2.5 V.

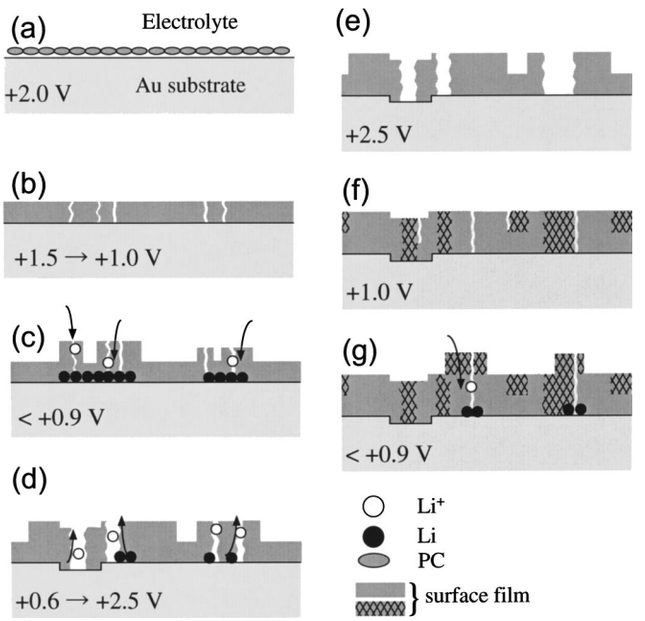

Figure 4. The schematic model of the formation and the change of the surface film on a gold electrode in PC solution containing 0.1 M $LiClO_4$ during two potential scan cycles: (a) at 2.0 V; (b) between 1.5 and 1.0 V; (c) at potentials more negative than 0.9 V; (d) during anodic stepping to 2.5 V; (e) at 2.5 V of the second potential scan cycle; (f) at 1.0 V; and (g) at potentials more negative than 0.9 V.

Acknowledgment

This work was partially supported by a Grant-in-Aid for Scientific Research (13554026) from the Ministry of Education, Culture, Sports, Science and Technology, Japan.

Hokkaido University assisted in meeting the publication costs of this article.

References

1. D. Fauteux and R. Koksbang, *J. Appl. Electrochem.*, **23**, 1 (1993).
2. E. Peled, *J. Electrochem. Soc.*, **126**, 2047 (1979).
3. E. Peled, in *Lithium Batteries*, J. P. Gabano, Editor, Academic Press, London (1983).
4. I. Yoshimatsu, T. Hirai, and J. Yamaki, *J. Electrochem. Soc.*, **135**, 2422 (1988).
5. D. Aurbach, I. Weissman, A. Zaban, and O. Chusid (Youngman), *Electrochim. Acta*, **39**, 51 (1994).
6. A. N. Dey and C. R. Schlaikjer, in *Proceedings of the 26th Power Sources Symposium*, Atlantic City, NJ, 1975, p. 47.
7. D. Aurbach and Y. Cohen, *J. Electrochem. Soc.*, **143**, 3525 (1996).
8. A. T. Ribes, P. Beaunier, and D. Lemordant, *J. Power Sources*, **58**, 189 (1996).
9. D. Aurbach, Y. Gofer, and Y. Langzam, *J. Electrochem. Soc.*, **136**, 3198 (1989).
10. O. Youngman, Y. Gofer, A. Meitav, and D. Aurbach, *Electrochim. Acta*, **35**, 625 (1990).
11. D. Aurbach and Y. Cohen, *J. Electrochem. Soc.*, **144**, 3355 (1997).
12. K. Kanamura, S. Shiraishi, and Z. Takehara, *J. Electrochem. Soc.*, **143**, 2187 (1996).
13. Y. S. Cohen, Y. Cohen, and D. Aurbach, *J. Phys. Chem. B*, **104**, 12282 (2000).
14. S. Shiraishi, K. Kanamura, and Z. Takehara, *J. Phys. Chem. B*, **105**, 123 (2001).
15. D. Aurbach, M. Daroux, and E. Yeager, *J. Electroanal. Chem. Interfacial Electrochem.*, **279**, 225 (1991).
16. D. Aurbach, M. Moshkovich, Y. Cohen, and A. Schechter, *Langmuir*, **15**, 2947 (1999).
17. A. Zaban and D. Aurbach, *J. Power Sources*, **54**, 289 (1995).
18. D. Aurbach and A. Zaban, *J. Electrochem. Soc.*, **141**, 1808 (1994).
19. T. Saito and K. Uosaki, *J. Electrochem. Soc.*, In press.
20. J. Clavilier, *J. Electroanal. Chem. Interfacial Electrochem.*, **107**, 205 (1980).
21. Y. Mo, Y. Gofer, E. Hwang, Z. Wang, and D. A. Scherson, *J. Electroanal. Chem.*, **409**, 87 (1996).

22. D. Aurbach and H. Gottlieb, *Electrochim. Acta*, **34**, 141 (1989).
23. N. Yamamoto, H. Hirasawa, H. Ishida, T. Tatsuma, and N. Oyama, *Bull. Chem. Soc. Jpn.*, **67**, 1296 (1994).
24. D. Aurbach and A. Zaban, *J. Electroanal. Chem.*, **393**, 43 (1995).
25. D. Aurbach and A. Zaban, *J. Electrochem. Soc.*, **142**, L108 (1995).
26. H. Li, Y. Mo, N. Pei, X. Xu, X. Huang, and L. Chen, *J. Phys. Chem. B*, **104**, 8477 (2000).
27. K. Naoi, M. Mori, and Y. Shinagawa, *J. Electrochem. Soc.*, **143**, 2517 (1996).